Ultrasensitive Refractive Index Sensor Based on Mach–Zehnder Interferometer and a 40μm Fiber

Xueqin Lei, Xiaopeng Dong, Tong Sun, and Kenneth T. V. Grattan

***Abstract*—An ultra-high sensitivity refractive index (RI) sensor, based on an in-line fiber Mach–Zehnder interferometer (MZI) and utilizing a special 40 μm fiber which has been specifically designed for the purpose, supporting only the LP_{01} and LP_{11} modes propagating in the fiber, has been proposed and numerically demonstrated in this work. The all-fiber MZI, based on LP_{01} and LP_{11} mode interference, was fabricated by utilizing a special design with two gradually tapered joints at both sides of this multi-clad thin diameter fiber (TDF). When the TDF diameters varied from 40 μm to 5 μm, a sudden change in the direction of the wavelength shift in the transmission spectrum of the TDF-MZI devices was observed both in liquid RI and air relative humidity (RH) monitoring experiments, as the surrounding RI or RH was seen to increase monotonically. Ultra-high sensitivity values of 5942.8nm/RIU (1.335-1.342) and 21292.2nm/RIU (1.4000–1.4025) were obtained in the experiments carried out, through the use of a tapered TDF-MZI device with TDF diameters of $\sim$5 μm and $\sim$9 μm, respectively. The maximum RH sensitivity of 1.084nm/%RH was obtained by the use of the TDF-MZI device with a TDF diameter of $\sim$12 μm. A compact all-fiber TDF-MZI sensor was thus created with an overall sensing length of $<$4mm, showing the advantages of high sensitivity, low loss, and flexibility in the tunable monitoring direction of the wavelength shift. This design is well suited to various applications, where the high sensitivity RI and RH measurements are required at precise locations.**

***Index Terms*—Dual mode fiber, fiber sensor, Mach-Zehnder interferometer, pressure, temperature.**

I. Introduction

OPTICAL fiber sensors have been widely investigated given the significant potential applications they have for measurements of parameters such as gas and liquid concentrations, compound material solidification monitoring, and biomolecule detection – all areas where the sensing of the surrounding refractive index (SRI) may be used as the underlying monitoring principle [1],[2]. In recent years, the fiber in-line Mach-Zehnder interferometers (MZIs) based on the "evanescent field" have been attracting increasing research interest, due to their inherent advantages of high sensitivity, compactness and flexibility in their design. The fabrication of an all-fiber in-line MZI "evanescent sensor" is thus dependent on the design of two special splitting/coupling interfaces along the fiber length. Components such as two identical heterogenic fibers [3], abnormal splicing points [4] or laser micro-machined grating arrangements [5] are used to excite the high-order/cladding modes propagating in the sensing fiber. However, the sensitivities obtained in those sensors were relatively low due to a weak interaction of the light beam with the surroundings. As reported by Jiang *et al.* and Li *et al.* [6], [7], the precision devices (e.g. a *fs* laser) have been used for the fabrication of microstructures in the fiber core/cladding to form an all-fiber MZI sensor, to allow high sensitivity RI measurements, with faster response and better spatial resolution [8]. However, potentially large losses and light scattering may be caused in a MZI structure with a complete opened path or side-ablated fiber core (with several abrupt heterogeneous interfaces between the silica and air created in the light path), due to the light propagating in the air or the liquid solutions directly, without experiencing the optical waveguide confinement occurring in a circularly symmetric fiber structure.

By contrast, micro- or nano-fiber show more promising optical properties of low transmission loss, a large evanescent field and tight optical confinement, beneficial for designing a high RI-sensitive fiber sensor [9], [10]. However, when the fiber required was tapered, by using a heating and pulling approach, the diameter of the fiber core will also gradually decrease, which increase the number of the high-order modes propagating in the sensing fiber and also create a "cutoff" of the core mode [11], which was then transformed to several cladding modes [12]. Moreover, the high temperature used ($\sim$2000K) is required to melt the silica fiber and make it suitable for drawing; however, achieving a steady temperature gradient in the heating region is difficult when using a flame [13]. Further, the lengths of the microfibers were enlarged by using a laser or a flame heating and drawing method [2][14–16], which may not be optimum for fabricating a compact sensor. The adiabatic conditions required for the taper transitions need to be carefully controlled to avoid the wavelength fluctuations, which may produce by multimodal interactions. Compared to using the 'heating and pulling' method, the size of the fiber core will not be changed

Manuscript received August 17, 2020; revised April 4, 2021; accepted June 3, 2021. Date of publication June 7, 2021; date of current version September 13, 2021. This work was supported by the National Natural Science Foundation of China under Grant 61775186, in part by the Fujian Provincial Department of Science and Technology under Grant 2014H6027, and in part by the Marine and Fisheries Bureau of Xiamen under Grant 16CZB025SF03. The work of Tong Sun and Kenneth T. V. Grattan was supported by the Royal Academy of Engineering. *(Corresponding authors: Xiaopeng Dong; Kenneth T. V. Grattan.)*

Xueqin Lei and Xiaopeng Dong are with the Institute of Lightwave Technology, School of Electronic Science and Engineering, Xiamen University, Xiamen 361005, China (e-mail: 23120160154507@stu.xmu.edu.cn; xpd@xmu.edu.cn).

Tong Sun and Kenneth T. V. Grattan are with the School of Mathematics, Computer Science and Engineering, City, University of London, EC1V 0HB London, U.K. (e-mail: t.sun@city.ac.uk; grattan@city.ac.uk).

using a chemical etching process unless the core region has been etched, which is better for the stable transmission of the core modes in the sensing fiber. Further, a chemical etching method could be used to form a compact microfiber, over a much shorter length (and thus better fitted for use for sensing at a precise location) that then could be readily fabricated by changing the size of the droplet of the etching chemical used, located using a fine injection head. This allows a much smaller diameter to be achieved (thus making it easier to achieve the high sensitivity needed) and that could be more easily controlled by changing the etching time and concentration of chemical solution used [17].

However in the MZI, which based on using the cladding modes, an amount of fiber cladding material of the sensing fiber to be etched remaining may cause a large transmission loss of the high-order/cladding modes that propagate in the fiber cladding: this leads to a decrease in the contrast of the interference fringes or even the disappearance of the periodic fringes. A similar case also has been seen in the MZI design based on etched few-mode fiber (FMF) [18], which was specially designed with the second highly-doped inner cladding to support only the fundamental mode and LP_{02} mode, propagating in the fiber. Firstly, the sensitivity of the FMF-MZI sensor, based on interference of fundamental mode and LP_{02} modes, was barely enhanced when the fiber diameter was reduced from 125 μm to 30 μm, which may increase the complexity and difficulty of the fabrication of a compact MZI sensor (with a FMF length of $\sim$20cm being employed) and thus designed for high sensitivity RI measurements. This is needed because a high degree of uniformity of the etched FMF diameter was required to support the circular symmetric third high-order mode, LP_{02}, propagating in the fiber. Secondly, when the fiber diameter was reduced to the second inner cladding of the FMF ($\sim$20 μm), the LP_{02} mode tended to cutoff, especially on the long wavelength side, which resulted in an upper limit of the RI sensitivity of 140nm/RIU (1.316-1.383) and 2489nm/RIU (1.433-1.439), respectively. Such a limit of RI sensitivity also exists in those MZI devices using microstructure sensing fibers with mutiple eccentric cores or air holes regions (e.g., photonic crystal fiber (PCF) [19], multi core fiber(MCF)[20] and twin core fiber (TCF) [21], etc.). The sensitivities (from a few tens, to one or two thousands nm/RIU) of those sensors are still inadequate for many critical applications, particularly so in bio-sensing which requires the accurate detection of an extremely small range of variations of the surrounding refractive index (SRI).

In this paper, a compact microfiber-assisted in-line MZI sensor has been proposed for ultrasensitive refractive index (RI) measurement, utilizing a special 40 μm thin diameter fiber (TDF) which supports only the foundational mode, LP_{01}, and the first high-order core mode, LP_{11}, propagating in the fiber. The design of the splicing and coupling joints of the MZI, with two gradually tapered points at both sides of TDF, was taken to form an in-line MZI and support only two core modes (LP_{01} and LP_{11}) interference. The sensing characteristics of the TDF-MZI devices, created using different TDF diameters which varied from 40 μm to 5 μm, have been theoretically and experimentally studied in this work. This all-fiber TDF-MZI sensor, taking advantages of both the use of microfiber and a compact fiber in-line MZI interferometer, also allows several advantages over these alternative approaches to be shown, which include: a) an ultrahigh sensitivity is characteristic of these sensors, where the maximum RI sensitivity of 21292.2nm/RIU obtained in our experiments is 1-3 orders of magnitude larger than is seen in a similar, chemical etched MZI device based on cladding mode interference or using a microstructure fiber; b) it uses relatively low optical loss and high stability in the transmission of the light, when compared to the other all-fiber in-line MZI devices, based on higher-order or cladding mode interference; c) it is simple, compact and only tiny amounts of analyte are required for high sensitivity measurements using the TDF-MZI sensor, with the sensing length required being less than 4mm; d) it is flexible for various applications, where tunability in the fiber diameter, sensitivity and direction of the wavelength shift in the transmission spectrum are required; e) it is suitable for use in both liquid and gaseous media, without requiring the use of any coating materials, where a capability to measure the air humidity has been also developed in this work using this TDF-MZI design. Thus the all fiber sensor discussed shows highly promising and significant prospects for use in making high sensitivity, RI-related measurements at a precise position, and is well suited to a wide variety of practical applications.

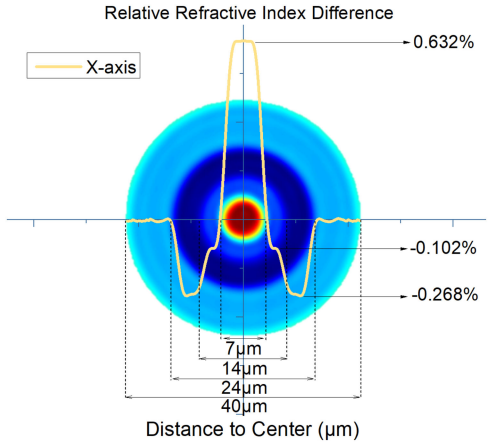

Fig. 1. Geometrical structure and refractive index difference profile (@632.8nm) of the 40μm (TDF). The parameters used in the simulation are: dco = 7 μm, Δnco = 0.632%, dcl1 = 14 μm, Δncl1 = $-$0.102%, dcl2 = 24 μm, Δncl2 = $-$0.268%.

II. Operational Principle of the Sensor

The TDFs used in the experimental work carried out were provided by the Yangtze Optical Fiber and Cable Limited Company Ltd, and specially designed using a GeO_2-doped inner core, two F-doped inner claddings and a pure silica outer cladding, with corresponding diameters of 7 μm, 14 μm, 24 μm and 40 μm, respectively, to ensure that only the LP_{01} and the LP_{11} modes were propagating along the fiber. The multi-layer geometrical structure and the W-shaped relative index difference profile (observed at a wavelength of 632.8nm) of the TDF used in the simulation are shown in Fig. 1, this being measured by using a SHR-1602, 3D refractive index profile device for optical fiber,

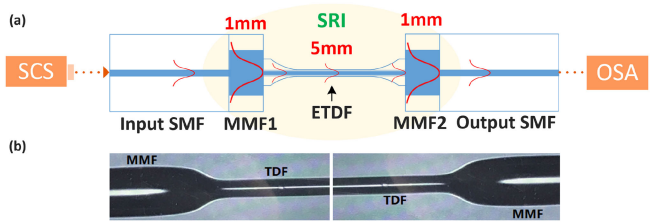

Fig. 2. (a) Schematic diagram of the fiber TDF-based MZI sensor. (b) Microscopic image of the TDF-MZI fiber structure after splicing. SCS – Supercontinuum laser source; OSA – Optical spectrum analyzer; SMF – Single mode fiber; MMF – Multimode fiber; TDF – Thin diameter fiber; ETDF – Etched thin diameter fiber.

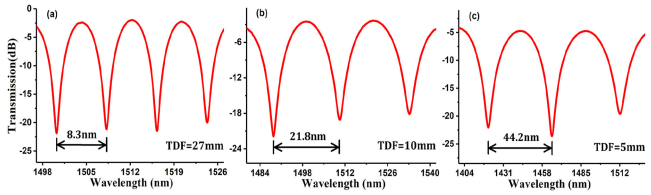

Fig. 3. Experimental transmission spectra of TDF-MZI sensor, with the following different lengths of TDF: (a) 27mm; (b) 10mm; (c) 5mm.

developed by the Key Laboratory of Specialty Fiber Optics and Optical Access Networks, Shanghai University.

As shown in Fig. 2(a), the all fiber in-line MZI used in this work were fabricated by splicing the TDF between two segments of the MMFs used, and the clear interference spectra for the TDF-MZIs with high extinction ratio (∼20dB) were obtained in the experiment, as shown in Fig. 3. The Free Spectral Range (FSR) of the periodic interference spectrum can be expressed as $FSR = \lambda^2/(\Delta n_{eff} L)$. Here L is inversely proportional to the FSR of a particular wavelength, for the transmission spectra of the TDF-MZI with different lengths of TDF (27mm, 10mm and 5mm). The shorter length of the TDF shows a larger FSR of the interference fringes, i.e., a wider wavelength range for the measurement which is good for avoiding the multi-value problem. Therefore, the fiber length for the TDF was chosen to be ∼5mm in the experiment to achieve a high sensitivity in the measurement – which may produce a large shift (per RIU) of the resonant wavelength.

The first high-order mode, LP_{11}, that propagate in the TDF was excited by the fundamental core mode, LP_{01}, in the input MMF_1. The interference between the LP_{01} and LP_{11} modes was selected by using the output MMF_2. If the optical power ratios transferred from the input SMF to the LP_{01} and LP_{11} modes are $t_{01} = P_{01}/P_{in}$ and $t_{11} = P_{11}/P_{in}$, respectively, then the transmission through the TDF is given simply as follows [22]:

$$T = P_{out}/P_{in} = t_{01}^2 + t_{11}^2 + 2t_{01}t_{11}\cos(\varphi(\lambda)) \quad (1)$$

where $\varphi(\lambda) = \Delta\beta(\lambda)L$ is the phase difference developed between the LP_{01} and LP_{11} modes in the TDF with a physical length, L, and $\Delta\beta = \beta_{01} - \beta_{11}$ is the propagation constant difference between the LP_{01} and LP_{11} modes. The phase difference between the LP_{01} and LP_{11} modes is a function of both the operating wavelength, λ, and the perturbation parameter, n_{SRI}(the

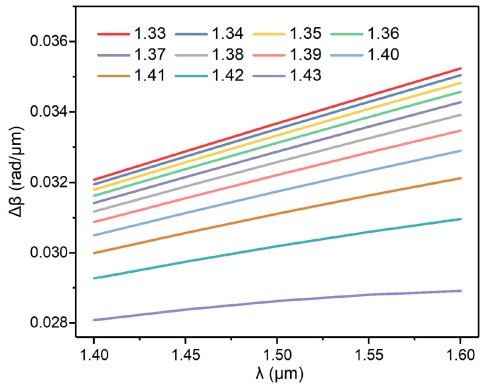

Fig. 4. Simulated results for $\Delta\beta$ of the LP_{01} and LP_{11} modes propagating in the TDF with the fiber diameter of 9 μm, under different SRI ranges from 1.33 to 1.43, as a function of wavelength.

refractive index of the surrounding material). Therefore, the change in the phase difference can be expressed as:

$$\Delta\varphi = \frac{\partial\varphi}{\partial n_{SRI}}\Delta n_{SRI} + \frac{\partial\varphi}{\partial\lambda}\Delta\lambda \quad (2)$$

When $\Delta\varphi = 0$, the RI sensitivity can be derived from Eq.(2):

$$\frac{\Delta\lambda}{\Delta n_{SRI}} = -\frac{1}{L}\left(\frac{\partial\varphi}{\partial n_{SRI}}\right)\left(\frac{\partial(\Delta\beta)}{\partial\lambda}\right)^{-1} \quad (3)$$

where $\frac{\partial\varphi}{\partial n_{SRI}} = \frac{\partial\Delta\beta}{\partial n_{SRI}}L$, and then the Eq.(3) can be shown as follows:

$$\frac{\Delta\lambda}{\Delta n_{SRI}} = -\left(\frac{\partial(\Delta\beta)}{\partial n_{SRI}}\right)\left(\frac{\partial(\Delta\beta)}{\partial\lambda}\right)^{-1} \quad (4)$$

Therefore, the RI response of the TDF-MZI only depends on the values of $\partial(\Delta\beta)/\partial n_{SRI}$and $\partial(\Delta\beta)/\partial\lambda$but not the length of sensing fiber. The COMSOL simulation software and the use of the finite element analysis approach were applied in this work for the calculation of the values of $\Delta\beta$ for the LP_{01} and LP_{11} modes propagating in the TDF, with a diameter of 9 μm, under the different surrounding refractive index (SRI) conditions shown in the Fig. 4. With the increase of SRI, the value of $\partial(\Delta\beta)/\partial\lambda$ becomes positive and decreases and thus the value of $(\partial(\Delta\beta)/\partial\lambda)^{-1}$increases. Moreover, the difference in the changes in $\Delta\beta$ increases as SRI increases, so that the value of $\partial(\Delta\beta)/\partial n_{SRI}$ increases. Therefore, the resonant wavelengths of peaks/dips in the transmission spectrum will shift monotonically, with the increase of SRI, and the sensitivity of the TDF-MZI will increase when the SRI becomes close to the RI of the fiber material.

When the diameter of the TDF ranges from 40 μm and 5 μm, the relationships obtained between the effective refractive index (ERI) of two core modes and the wavelength (at a temperature of 25 °C) have been studied in this work. In the simulation carried out, a liquid of known SRI (e.g., 1.4) is used and coated around the TDF. The simulation has shown that the etched TDF can still support the LP_{01} and LP_{11} modes propagating in the fiber, when the fiber is used in an aqueous medium. As shown in Fig. 5(a), the LP_{01} mode is seen as stable until the diameter of the TDF reduces to a value of 24 μm (corresponding to the

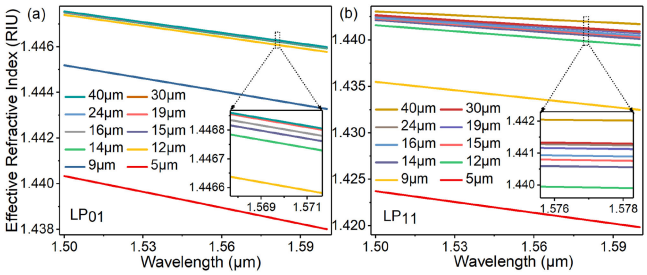

Fig. 5. Calculated ERI of (a) the LP_{01} mode and (b) the LP_{11} mode propagating in the TDF, as a function of wavelength, under the change of the fiber diameters ranging from 40 μm to 5 μm.

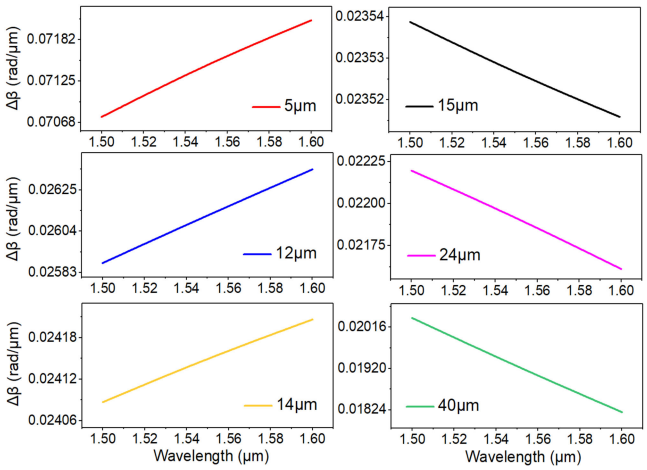

Fig. 6. Calculated $\Delta\beta$ of two core modes propagating in the TDF, as a function of wavelength, under the different diameters of TDF ranging from 40 μm to 5 μm.

second cladding diameter of TDF), and then changes slightly over the diameter range from 24 μm to 14 μm (corresponding to the second cladding of the TDF). The value of n_{eff}^{01} changes rapidly when the diameter of the TDF is reduced to $<$14 μm (corresponding to the first cladding diameter of the TDF). As shown in Fig. 5(b), the LP_{11} mode exhibits a relatively larger difference of n_{eff}^{11}, when the diameter of the TDF changes from 40 μm to 5 μm, and a similar sudden change develops in the variation of n_{eff}^{11} vs. wavelength, when the diameter of the TDF is reduced to 14 μm, which may result in a corresponding variation of $\Delta\beta$ between the interference of the LP_{01} and LP_{11} modes in the TDF-MZI.

As shown in Fig. 6, the value of $\partial(\Delta\beta)/\partial\lambda$ is positive when the diameter of the TDF is set in the range 5 μm $\sim$ 14 μm, while it is negative when the diameter of the TDF ranges over 15 μm $\sim$ 40 μm. Thus when the diameter of the TDF was reduced to 14 μm (related to the first cladding area of the TDF), a sudden change of the direction of the wavelength shift in the transmission spectrum of the LP_{01} and LP_{11} mode interference in the TDF-MZI sensor could be seen, as the value of the SRI is increasing. Further, the thinner diameter of the TDF with a larger $\Delta\beta$ of the LP_{01} mode and the LP_{11} mode propagating in the fiber, will contribute to the larger variation of the phase difference seen, as well as the higher sensitivity in RI measurements of liquids surrounding it. All the samples studied with different TDF diameters exhibited good monotonic relationships with $\Delta\beta$, over wavelengths ranging from 1400nm to 1600nm, as has been studied in this work. The tunability of the sensitivities and the directions of the wavelength shift in the interference spectrum of the LP_{01} and LP_{11} modes increases the flexibility in the optimization of the sensitivity and the measurable wavelength range of the TDF-MZI sensor. Thus the TDF-MZI sensor proposed in this work is very promising in its application to measuring the RI, with high sensitivity, at a precise position and this shows a good adaptability as a practical solution to different measurement applications.

III. Fabrication of the TDF Based MZI Sensor

The experimental setup employed in the SRI measurement scheme and the configuration of the TDF-based MZI used is shown in Fig. 2(a). The TDF-MZI was formed easily by splicing a section of the TDF between two pieces of step-index multimode fibers (MMFs). The core/cladding diameters of the standard SMFs (Corning SMF-28) and MMFs used in this work are 8.2/125μm and 62.5/125μm, respectively. In the experiment undertaken, the splicing operation between the SMFs and the MMFs was performed by using an automatic fusion splicer (Ruiyan, RYF600P). The splicing operation between the TDF and the MMF was, however, performed by using the manual mode of a fusion splicer (DVP-720A), setting the splicing parameters to a low discharge power (80bit) and a short discharge time (60ms). Further, the stripper and cutter used in this work were special adjusted to suit the 40 μm TDF. In order to avoid bending and deformation of the thin diameter fiber, the arc discharge position was specially adjusted for splicing the TDF to the MMFs, allowing a small deviation distance ($\sim$60 μm) from the splicing point to the side of the MMFs. Due to the large difference in the fiber diameters between the MMFs and the TDF, the splicing points of the TDF and the MMFs were slightly tapered, as shown in the Fig. 2(b). The gradually tapered joints formed allow light to propagate easily in the core of the MMF_1, then to couple into the fiber core of the TDF, and then back again to the core of the MMF_2. Without the MMFs used in this work, an offset of the fiber cores – between the SMFs ($\sim$8.2μm) and TDF ($\sim$7μm) – may occur in the manual splicing process. Therefore, the use of two segments of MMFs in this work is important for the stimulation of the core modes (the LP_{01} and the LP_{11} modes) on a symmetrical basis, when these propagate in the sensing fiber. To do so greatly enhances the stability and repeatability needed to fabricate reliable, in-line fiber optic-based TDF-MZI devices.

To develop the required sensitivity of the TDF sensor to the RI of the surrounding liquid, part of the TDF cladding was removed by chemical etching with buffered hydrofluoric acid (BHF) solution (this being a mixture of hydrofluoric acid solution (HF, 40wt.%), ammonium fluoride (NH4F), and deionized water (H_2O)). The TDF-MZI was placed in a flat polymer box, and to keep it straight, it was fixed with a polymer adhesive. Due to the large difference in the fiber diameters between the MMFs and the TDF, the sensing fiber was suspended in the air. Then the fine injection head (of 0.23 mm diameter) was used in the experiment to obtain a single droplet that was dripped onto the surface of the

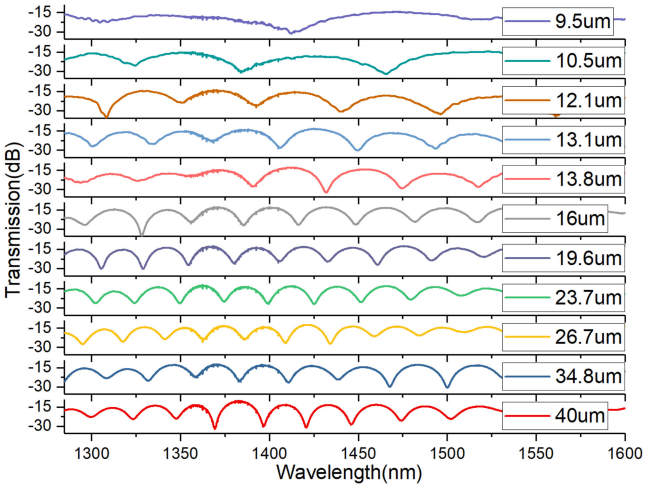

Fig. 7. Experimental transmission spectra of a TDF-MZI sensor during the process of chemical etching, as the diameter of TDF is reduced from 40 μm to 9.5 μm. (TDF: the whole fiber length ∼8mm and the middle etched area <7mm).

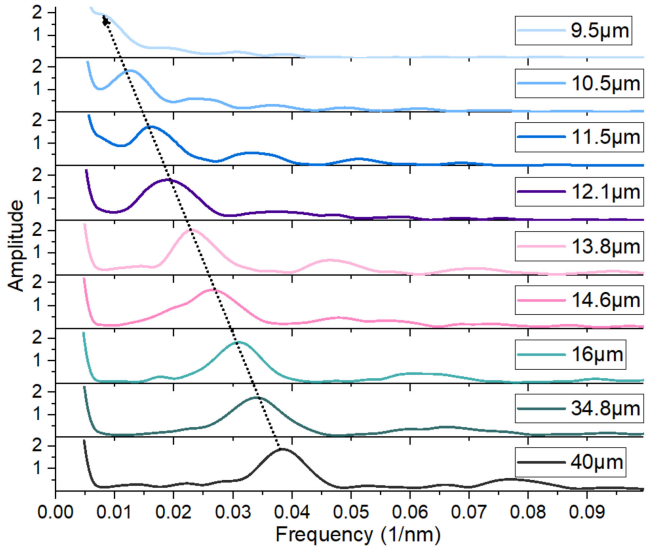

Fig. 8. Fourier transformation of interference spectra of the TDF-MZI sensor, when the diameter of TDF is decreasing over the range shown.

TDF. During the process of chemical etching, the air velocity was controlled by using a fume hood and a tunable air vent on the etching box, to allow the air to enter and escape. In that way, the TDF was slightly tapered, due to the slow evaporation of the BHF solution. At both sides of the TDF in the MZI, the distance from the droplet of BHF to the splicing joints of the TDF-MMFs was taken, and thus the length of tapered region created was less than 4mm. The length of the tapered region could be further reduced by using an injection head with a smaller diameter, to form a more compact fiber MZI device, which then could be used for RI measurements at a precise position.

In the experiment carried out, the transmission spectrum of a TDF-MZI with the fiber length of TDF about 8mm was monitored during the process of chemical etching, as shown in Fig. 7. When the diameter of the TDF was required to be reduced from 40 μm to 9.5 μm, the interference spectrum of the TDF-MZI was stable in the BHF solution, with the increase of the period of the interference between the LP_{01} and LP_{11} modes propagating in the TDF. Thus a wide wavelength range for the TDF-MZI was created with a limited FSR, to allow high sensitivity measurements, for a defined physical diameter of the TDF. The contrast of the interference fringes decreases from ∼20dB to ∼16dB, due to the change of the energy ratio between the LP_{01} mode and the LP_{11} mode propagating in the sensing fiber, as the TDF diameter varies from 40 μm to 9.5 μm. The corresponding Fast Fourier Transformation (FFT) of the interference spectra of the TDF-MZI sensor, as the diameter of the TDF was decreasing, is shown in the Fig. 8. It can be seen that there is indeed one dominant, high order mode, which means that two main interference modes are seen and decide the interference spectrum. The frequency of the two main interference modes is evident and gets closer to zero as the diameter of TDF was reduced to a small size. The shift in the frequency of the two main mode interference, varying as the diameter of the TDF decreases, can be illustrated by the change of the value of Δn_{eff} between the LP_{01} and the LP_{11} modes, this being due to the regions of fiber cladding materials removed by the chemical etching being replaced by the BHF solutions.

IV. Experimental Results and Discussion

In the experiment carried out, the TDF-MZI sensor thus created was connected to a supercontinuum laser source (SC-5, YSL Co. Ltd. operating over the wavelength range 480-2400nm). This was deployed as a broadband light source in this experiment, and an Optical Spectrum Analyzer (OSA, ANDO AQ6317B) with a resolution of 0.01nm was used to record the transmission spectrum of the TDF-MZI sensor. The refractometer (KEM RA-130), with a resolution of 0.0001, was used for measurement and calibration of the RI value of the test solutions, and the SRI testing experiments were undertaken at room temperature, 22 °C. The sensing structures of the TDF-MZIs were kept straight and surrounded by the droplets of the sucrose solutions under study. The sensors were cleaned with ethyl alcohol and completely dried to remove any residual liquid before each test was carried out. The spectral responses of the TDF-MZI with a TDF diameter of D = 9 μm were monitored using test solutions with the different RI ranges shown in Fig. 9. The results show that the spectral dip moves monotonically toward longer wavelengths, as the SRI is increasing, and maximum RI sensitivity values of 21292.2 nm/RIU, 11993.3 nm/RIU, and 3312.4 nm/RIU, in the measuring ranges of 1.4000–1.4025, 1.3700–1.3740 and 1.336–1.344, were respectively obtained in these experiments. Considering the wavelength resolution of the OSA used (0.01 nm), the RI sensor with D = 9 μm has RI resolution values of 4.7×10^{-7} (RI = 1.4000–1.4025), 8.3×10^{-7} (RI = 1.3700–1.3740) and 3.02×10^{-6} (RI = 1.336–1.344) which, to the best of our knowledge, are significantly higher than have previously been reported, as shown in Table I.

Further RI evaluation tests of the performance of the TDF-MZI sensors were undertaken using different diameters of the sensing fiber. In these experiments, the diameter of sensing fiber

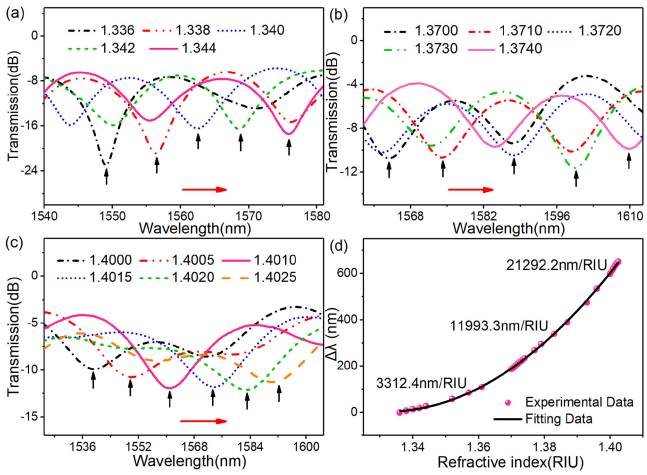

Fig. 9. Measured spectral responses of an etched TDF-MZI structure with D = 9 μm over different SRI ranges: (a) 1.336–1.344, (b) 1.3700–1.3740, and (c) 1.4000–1.4025, (d) wavelength shift versus SRI.

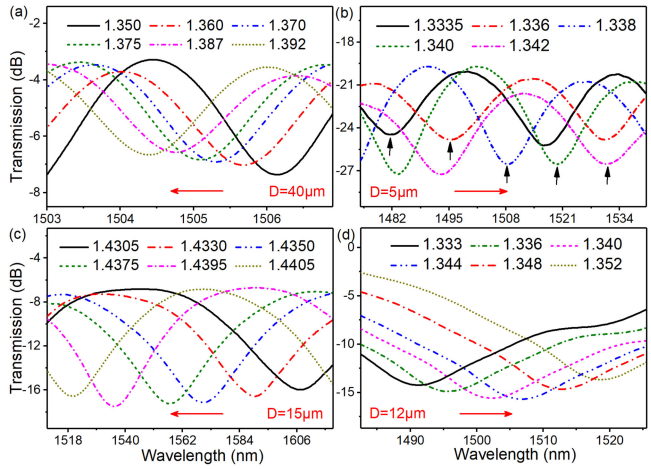

Fig. 10. Measured spectral responses of an etched TDF-MZI structure with the different diameters of TDF: (a) 40 μm; (b) 5 μm; (c) 15 μm; (d) 12 μm.

TABLE I
TYPICAL RI SENSITIVITIES OF DIFFERENT FIBER-OPTIC RI SENSING SCHEMES

Type of sensor	Sensing head length (mm)	Maximum RI sensitivity (nm/RIU)	SRI range	Type of modes	Ref.
FPI based on etched MCF and CFBG	14	1.43	1.316-1.324	Core modes in different cores	[20]
Two-arms MZI based on tapered MMF	12	2576	1.337-1.340	HE_{11} and HE_{12} modes	[16]
In-line MZI based on etched PCF	35	359	1.333-1.381	Core mode and cladding modes	[19]
In-line MZI based on tapered PCF	24	1629	1.333-1.351	Core mode and cladding modes	[15]
In-line MZI based on etched TCF	80	130	1.338-1.364	Core mode and cladding modes	[21]
		351	1.384-1.398		
In-line MZI based on etched FMF	200	140	1.316-1.383	LP_{01} and LP_{02} modes	[18]
		2489	1.433-1.439		
In-line MZI based on etched 40μm TDF	7	5942	1.335-1.342	LP_{01} and LP_{11} modes	This work
		21292	1.400-1.4025		

(TDF) used varied from 40 μm to 5 μm, using chemical etching to achieve the different values used. The interference of the LP_{01} and LP_{11} modes was then formed in the TDF-MZI sensor and was stable in the aqueous solutions used. The TDF-MZI sensors with TDF diameters of D = 12 μm and D = 5 μm, respectively, exhibit different spectral responses: however, the directions of the wavelength shift with the increase of SRI were the same, as shown in Fig. 10(b) and Fig. 10(d). By contrast, the TDF-MZI sensors with TDF diameters of D = 15 μm and D = 40 μm, respectively, exhibit wavelength shifts in the opposite directions, with increasing SRI, as shown in Fig. 10(a) and Fig. 10(c). A large numbers of experimental studies of TDF-MZI devices with a TDF length of 4mm and the tapered TDF diameter varying from 40 μm to 5 μm have been developed, and studies of these reveal that the direction of the wavelength shift is related to the diameter of the TDF, as the SRI is increasing. As observed in the experimental results obtained, a demarcation point in the direction of the wavelength shift in the transmission spectrum was seen when the TDF diameter was tapered from 40 μm to 5 μm. The change happens over the tapered TDF diameter range from 15 μm-12 μm, which coincides with the results of the theoretical simulation carried out (with a sudden change in monotonicity of $\Delta\beta$ vs. wavelength happening at a 14 μm diameter of the TDF). With the reduction of the first cladding diameter of the TDF, the resonant dips shift to the longer wavelength region and this shows an ultrahigh sensitivity to the surrounding RI. Under this condition, the sensor can be seen as a thin cladding MZI structure, with the core modes propagating in the TDF fiber core, having a relatively strong interaction with the surroundings due to a large evanescent field created. When all the materials used in the fiber cladding were removed, the test solutions and air act as the "cladding" of the sensing fiber. The interference modes of the LP_{01} mode and LP_{11} mode could also be excited and propagate in the sensing fiber, due to the design of the splicing and coupling joints of the MZI with two gradually tapered points on both sides of TDF. Therefore, this special designed TDF-MZI sensor takes advantage of *both* the microfiber and all-fiber in-line MZI interferometer used.

Regardless of the different directions of the wavelength shift in the transmission spectrum, the relationship between the diameter of the TDF and the absolute RI sensitivity is shown in Fig. 11. Here, the maximum sensitivities for D = 5 μm, D = 9 μm, D = 12 μm and D = 19 μm, D = 23 μm and D = 40 μm are 5942.82nm/RIU (SRI = 1.335–1.342), 3436.78nm/RIU (SRI = 1.335–1.344), 1495.53nm/RIU (SRI = 1.336–1.352),

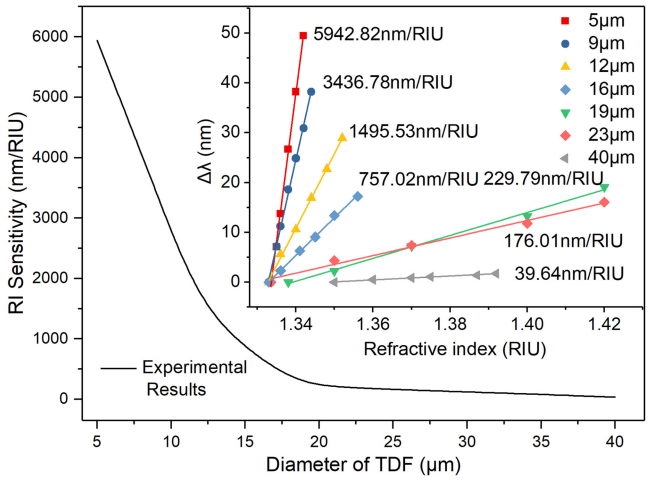

Fig. 11. Relationship between RI measurement sensitivity (absolute value) and the diameter of TDF used.

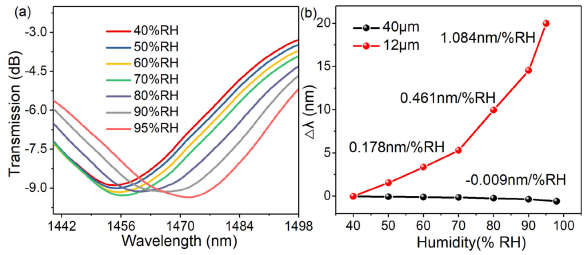

Fig. 12. (a) Measured transmission spectrum of an etched TDF-MZI sensor with a TDF diameter of 12 μm, as the RH range varies from 40%RH to 95%RH. (b) Relationship between wavelength shift and humidity for two TDF-MZI, with different TDF diameters of 40 μm and 12 μm.

229.79nm/RIU (SRI = 1.35–1.42), 176.01nm/RIU (SRI = 1.35–1.42), and 39.64nm/RIU (SRI = 1.36–1.392), respectively. As expected, the RI sensitivity *increases* as the TDF diameter *decreases*. For all the six samples studied, the linear correlative coefficients R^2 are greater than 0.995, which indicates that the wavelength shift observed exhibits a good, linear relationship with the SRI changes, over a small RI range. It is notable that the fiber with the thinner diameter shows a relatively larger difference in sensitivity over a wide measurement range of the SRI. In the experiment, higher sensitivity of the TDF-MZI can be realized with the use of a more uniform and thin sensing fiber, by optimizing the tapering process in the chemical etching. Further, a smaller size of the TDF-MZI sensor can be achieved by using a professional splicer and cutter to deal with the special 40 μm fiber. Thus the TDF-MZI sensor discussed in this work could then be used effectively in a range of measurement applications which have different requirements in terms of sensitivity and the methods of demodulation, pursuing a high fineness of interference fringes or tunability of the different directions of the resonant wavelength shift seen in the transmission spectrum.

Dispensing with the need for a coating for a relative humidity (RH) sensor is a very useful development, and given the increase in RI sensitivity of the sensor demonstrated already over what has been reported, the next stage is to explore whether it is possible to implement an RH sensor without the need for any additional humidity sensitive coatings on the fiber surface. To investigate this, in the experiment an RI sensor was placed in a commercial constant-temperature humidity test chamber (CK-80G, Qin Zhuo Co. Ltd) at normal air pressure, this having a RH measuring range from 20%RH to 98%RH and a temperature range from 0 °C to 150 °C. Both the humidity and temperature can be controlled separately using this system, which gives important flexibility in the calibration process. During the experiment carried out, the surrounding temperature was maintained at 22 $\pm$ 0.5°C to remove the influence of temperature variations, while increasing the RH.

When the surrounding RH was gradually increased from 30%RH to 98%RH, an obvious change in the transmission spectrum of the sample with a TDF diameter of 12 μm was detected and this is shown in Fig. 12(a). The direction of the wavelength shift with increasing RH is the same as the direction of the wavelength shift with increasing SRI, as shown in Fig. 10(d). The RI change of the air is the main reason that explains that the performance of the RH-induced spectral shift of the TDF-MZI sensor, over the relative low humidity range. The gas RI, n, is proportional to the gas density, ρ, which can be presented by the Gladsne–Dale relationship [23]: $(n-1)/\rho$ = constant. The variation in the density of the gas and the water molecules results in the ERI variations seen in the LP_{01} mode and LP_{11} mode, as well as leading to variations in the phase difference, φ. Moreover, different species of gas show relatively different RI values for the gas [24], which means that any small variation of the gas composition in the atmosphere may lead to a slight change in the RI of the air (but the change is small, at the level of fourth or fifth decimal place). On the other hand, since the TDF-MZI has a higher relative RI sensitivity over a relatively higher SRI range, as shown in Fig. 9, its response to the RI variation of the gas ($n \approx 1.0003$) is lower, comparatively than the for the water molecules present ($n \approx 1.333$). When considering the relatively higher humidity ranges used in the work, a thin film of moisture may be deposited on the fiber surface due to the condensation of water vapor. This will significantly increase the ERI of the interference modes propagating in the sensing fiber, due to the evanescent wave and lead to a larger RH-induced spectral shift, as shown in Fig. 12(a). Therefore, detecting the change in the density of the water molecules becomes the dominant mechanism of the "evanescent sensor" here, for humidity measurements.

Moreover, a comparison of the performance of the TDF-MZI sensor was made, with the sensing fiber diameters of 40 μm and 12 μm, in the RH monitoring experiments carried out. As can be seen in Fig. 12(b), the directions of the wavelength shift in transmission spectra of the TDF-MZI sensors (using the different sensing fiber diameters (D = 40 μm and D = 12 μm)) are different with increasing RH, which corresponds to the directions of the wavelength shift with increasing SRI, illustrated in Fig. 10(a) and Fig. 10(d). Thus a rapid change of the direction of the wavelength shift in the transmission spectrum of the LP_{01} and LP_{11} mode interference in the TDF-MZI sensor could be seen in *both* the RH and the RI measurements, and which agree

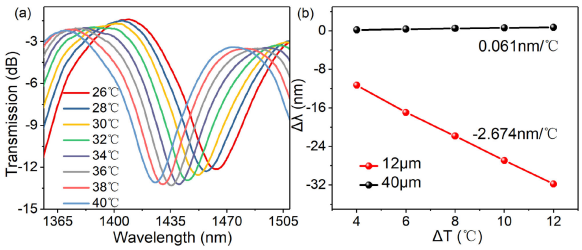

Fig. 13. (a) Measured transmission spectrum of an etched TDF-MZI sensor with the TDF diameter of 12 μm, as the temperature range varies from 26 °C to 40 °C. (b) Relationship between wavelength shift and temperature for two TDF-MZI, with different TDF diameters of 40 μm and 12 μm.

well with the simulation results reported in this work. Moreover, a larger RH sensitivity for the TDF-MZI sensor is obtained for a thinner sensing fiber diameter, especially when looking at the higher RH range. This is an important case where the sensitivity of the TDF-MZI sensor with a thinner sensing fiber diameter is particularly good, showing a larger difference across a wide range of RI values. Thus a RH sensitivity of 1.084nm/%RH was obtained (in the RH range 90%RH to 95%RH), which is over twenty-three times higher than that reported in previous work (-0.047 nm/%RH), based on a bare fiber structure without a hygroscopic coating layer [25]. It can be noted that in this reported work, it is ten times higher over than for the coated FBG ($\sim$0.0045nm%RH). Therefore, this compact TDF-MZI device based on two core mode interference, designed for RI *and* RH measurements – both having the characteristics of tunability of the sensitivity and direction of the wavelength shift in the transmission spectrum of the LP_{01} and LP_{11} mode interference.

In addition, the dependence of the resonant wavelength on temperature was examined by placing the TDF-MZI sensor in an electrically controlled water-filled oven (DC-0520, Zhu Lan Co., Ltd). The temperature of the water bath was gradually increased from 26 °C to 40 °C, and as the water temperature increases, the transmission spectrum of the TDF-MZI, with the TDF diameter of 12 μm, was obtained, as shown in Fig. 13(a). The temperature sensitivity of the TDF-MZI was tested at a TDF diameter of 40 μm and 12 μm, as shown in Fig. 13(b). The resonant wavelength of the response of the peaks/dips occurs linearly with the variation of the water temperature surrounding the sensing fiber. The temperature cross-sensitivity is 1.53×10^{-3} RIU/°C and -1.78×10^{-3} RIU/°C for the TDF diameters of 40 μm and 12 μm, respectively. A commercial thermometer (with a resolution of $\pm$0.1 °C) was used to monitor the temperature in the process of the RI or RH tests carried out. It should be noted that the temperature sensitivity of the TDF-MZI increased, as the diameter of TDF decreases, which benefits from the change of refractive index of the solution due to the temperature variation. Therefore, this high sensitivity RI sensing scheme has the potential to further developed into a highly effective, high sensitivity fiber temperature sensor.

V. Conclusion

In summary, the research reported has shown that an ultra-sensitive optical fiber sensor based on a compact TDF-MZI structure is both feasible and reliable for making RI and RH measurements. This design has the advantages of simplicity of structure, ease of fabrication, low cost and tunability of the sensitivity and directions of the resonant wavelength shift in the transmission spectrum. In experiments carried out, the all fiber TDF-MZI sensor reported exhibited a low measuring limit of 4.7×10^{-7} RIU, a high sensitivity of 21292.2nm/RIU and a good linearity of 99.8% over the important RI range from 1.4000 to 1.4025, using a sensing fiber diameter of 9 μm. The maximum RI sensitivity, of 5942.82nm/RIU over the measuring range from 1.335 to 1.342, could be achieved by using the TDF-MZI sensor with a TDF diameter of 5 μm. In addition, the in-line TDF-MZI sensor, with a tapered TDF (e.g. where D = 12 μm) could be configured as a high sensitivity RH sensor, having the advantage of no additional coating being needed on the surface of the sensing fiber. This TDF-MZI sensor has clear advantages in ultrahigh sensitivity measurements, located at precise positions, to monitor the RI and RH of surrounding materials. Such a device clearly has important practical applications in a number of areas, including fiber-optic bio- and chemical- sensing, and is suitable for use with both liquid and gaseous media.

References

[1] J. Villatoro and D. Monzon-Hernandez, "Low-cost optical fiber refractive-index sensor based on core diameter mismatch," *J. Lightw. Technol.,* vol. 24, no. 3, pp. 1409–1413, Mar. 2006.

[2] J. Wo *et al.*, "Refractive index sensor using microfiber-based Mach–Zehnder interferometer," *Opt. Lett.,* vol. 37, no. 1, pp. 67–69, Jan. 2012.

[3] L. Ying, G. F. Yan, and S. He, "Thin-core fiber sandwiched photonic crystal fiber modal interferometer for temperature and refractive index sensing," *IEEE Sens. J.,* vol. 18, no. 16, pp. 6627–6632, Jun. 2018.

[4] J. Yang *et al.*, "In-fiber Mach-Zehnder interferometer with piecewise interference spectrum based on hole-assisted dual-core fiber for refractive index sensing," *Opt. Exp.,* vol. 26, no. 15, pp. 19091–19099, Jul. 2018.

[5] Y. Tan, L-P. Sun, L. Jin, J. Li, and B-O. Guan, "Microfiber Mach-Zehnder interferometer based on long period grating for sensing applications," *Opt. Exp.*, vol. 21, no. 1, pp. 154–164, Jan. 2013.

[6] L. Jiang, L. Zhao, S. Wang, J. Yang, and H. Xiao, "Femtosecond laser fabricated all-optical fiber sensors with ultrahigh refractive index sensitivity: Modeling and experiment," *Opt. Exp.*, vol. 19, no. 18, pp. 17591–17598, Aug. 2011.

[7] Z. Li *et al.*, "Ultrasensitive refractive index sensor based on a Mach–Zehnder interferometer created in twin-core fiber," *Opt. Lett.,* vol. 39, no. 17, pp. 4982–4985, Sep. 2014.

[8] G. Brambilla *et al.*, "Optical fiber nanowires and microwires: Fabrication and applications," *Adv. Opt. Photon.,* vol. 1, no. 1, pp. 107–161, Jan. 2009.

[9] D. Liu *et al.*, "High sensitivity refractive index sensor based on a tapered small core single-mode fiber structure," *Opt. Lett.,* vol. 40, no. 17, pp. 4166–4169, Sep. 2015.

[10] K. Li, N. M. Y. Zhang, N. Zhang, T. Zhang, G. Liu, and L. Wei, "Spectral characteristics and ultrahigh sensitivities near the dispersion turning point of optical microfiber couplers," *J. Lightw. Technol.,* vol. 36, no. 12, pp. 2409–2415, Jun. 2018.

[11] J. D. Love *et al.*, "Tapered single-mode fibres and devices: I. Adiabaticity criteria," in *Proc. IEE J – Optoelectron.,* vol. 138, no. 5, pp. 343–354, Oct. 1991.

[12] R. J. Black and R. Bourbonnais. "Core-mode cutoff for finite-cladding lightguides," in *Proc. IEE J – Optoelectron.,* vol. 133, no. 6, pp. 377–384, Dec. 1986.

[13] L. Tong *et al.*, "Subwavelength diameter silica wires for low-loss optical wave guiding," *Nature*, vol. 426, no. 6968, pp. 816–819, Dec. 2003.

[14] S. Pu, L. Luo, J. Tang, L. Mao, and X. Zeng, "Ultrasensitive refractive-index sensors based on tapered fiber coupler with SAGNAC loop," *IEEE Photon. Technol. Lett.,* vol. 28, no. 10, pp. 1073–1076, May 2016.

[15] C. Li, S.-J. Qiu, Y. Chen, F. Xu, and Y.-Q. Lu, "Ultra-sensitive refractive index sensor with slightly tapered photonic crystal fiber," *IEEE Photon. Technol. Lett.,* vol. 24, no. 19, pp. 1771–1774, Oct. 2012.

[16] H. Luo, Q. Sun, Z. Xu, D. Liu, and L. Zhang, "Simultaneous measurement of refractive index and temperature using multimode microfiber-based dual Mach–Zehnder interferometer," *Opt. Lett.,* vol. 39, no. 13, pp. 4049–4045, Jul. 2014.
[17] M. F. Namiq and M. Ibsen, "Simple technique of determining the fibre diameter during etching," *Opt. Exp.*, vol. 26, no. 25, pp. 32908–32917, Dec. 2018.
[18] C. Lu, X. Dong, and J. Su, "Detection of refractive index change from the critical wavelength of an etched few mode fiber," *J. Lightw. Technol.,* vol. 35, no. 13, pp. 2593–2597, Jul. 2017.
[19] H. Du, X. Sun, Y. Hu, X. Dong, and J. Zhou, "High sensitive refractive index sensor based on cladding etched photonic crystal fiber Mach-Zehnder interferometer," *Photon. Sens.,* vol. 9, no. 2, pp. 126–134, Jun. 2019.
[20] S. G. Kilic, Y. Zhu, Q. Sheng, M. N. Inci, and M. Han, "Refractometer with etched chirped fiber Bragg grating Fabry–Perot interferometer in multicore fiber," *IEEE Photon. Technol. Lett.,* vol. 31, no. 8, pp. 575–578, Apr. 2019.
[21] C. Zhang *et al.*, "Etching twin core fiber for the temperature-independent refractive index sensing," *J. Opt.,* vol. 20, no. 4, Apr. 2018, Art. no. 045802.
[22] P. Lu and Q. Chen, "Asymmetrical fiber Mach Zehnder interferometer for simultaneous measurement of axial strain and temperature," *IEEE Photon. J.,* vol. 2, no. 6, pp. 942–953, Dec. 2010.
[23] J. H. Gladstone and T. P. Dale, "Researches on the refraction, dispersion, and sensitiveness of liquids," *Philos. Trans. Roy. Soc. London*, vol. 153, pp. 317–343, Jan. 1863.
[24] S. Pevec and D. Donlagic, "Miniature fiber-optic Fabry-Perot refractive index sensor for gas sensing with a resolution of $5x10^{-9}$ RIU," *Opt. Exp.*, vol. 26, no. 18, pp. 23868–23882, Sep. 2018.
[25] M. Shao, X. Qiao, H. Fu, N. Zhao, Q. Liu, and H. Gao, "An in-fiber Mach–Zehnder interferometer based on arc-induced tapers for high sensitivity humidity sensing," *IEEE Sens. J.*, vol. 13, no. 5, pp. 2026–2031, May 2013.

Xueqin Lei was born in Zhejiang Province, China, in 1990. She received the bachelor's degree in optical information science and technology and the master's degree in optics from Zhejiang Normal University, Zhejiang, China, in 2013 and 2016, respectively. She is currently working toward the Doctoral degree in electromagnetic field and microwave technology with Xiamen University, Xiamen, China. Her research interests include optical fiber interferometric sensor designing, fabricating, theoretical studying, and application in marine and industry.

Xiaopeng Dong received the bachelor's degree from Shandong University, Jinan, China, in 1983, and the master's degree from the University of Science and Technology of China (USTC), Hefei, China, in 1986.

In 1986, he joined the Faculty of USTC with the Department of Electronics Engineering and Computer Science. In 1998, he transferred from USTC to the Department of Electronics Engineering, Xiamen University, Xiamen, China, where he was promoted to a Full Professor, in 2000. He visited the Optoelectronics Research Center (ORC) with Southampton University, Southampton, U.K., from 1992 to 1993, the Department of Electronics Engineering, City University of Hong Kong, Hong Kong, from 1996 to1997, and the Department of Engineering Physics, McMaster University, Hamilton, ON, Canada, in 2004.

He has authored or coauthored more than 100 journal articles and conference papers and obtained more than ten patents. His research interests include special fibers and optical waveguides, fiber gratings-based components and sensors, interferometric fiber and waveguide devices and sensors, optical fiber current sensor, and optical fiber gas sensor.

Tong Sun received the B.Eng., M.Eng., and D.Eng. degrees in precision instrumentation from the Harbin Institute of Technology, Harbin, China, in 1990, 1993, and 1998, respectively, and the Ph.D. degree in applied physics from the City, University of London, London, U.K., in 1999.

She is currently the Director of the Photonics and Instrumentation Research Centre, City, University of London, and leads research in developing and applying optical fiber sensors and instrumentation to address topical industrial problems. She has authored or coauthored more than 300 scientific and technical papers in journals and in addition has given many keynote papers at main conferences. She is an inventor of eight patent applications. She is an Associate Editor for the *Measurement* (Elsevier) and a Guest Editor of the *Journal of Lightwave Technology*. She is on the Editorial Board of the *Journal of Sensor* and the *Journal of Optical and Quantum Electronics*. In 2020, she was elected to the Royal Academy of Engineering, as a Fellow. She was the recipient of the Silver Medal by the Royal Academy of Engineering, U.K., in 2016, and the Callendar Medal and the Oxburgh Medal by the Institute of Measurement and Control, U.K., in 2010 and 2016, respectively. She received the Officer of the Order of the British Empire by the Queen's 2018 Birthday Honours List for services to engineering in 2018.

Kenneth T.V. Grattan received the B.Sc. (Hons.) degree in physics from Queens University Belfast, Belfast, U.K., in 1974, the Ph.D. degree in laser physics in the use of laser-probe techniques for measurements on potential new dye laser systems, and the D.Sc. degree from City University, in 1992, for his work in sensor systems.

In 1978, he became a Research Fellow with the Imperial College of Science and Technology, London, U.K., to work on advanced photolytic drivers for novel laser systems. In 1983, he joined City, University of London, London, U.K., as a new blood Lecturer of physics, where he was appointed as a Professor of measurement and instrumentation in 1991, and the Head of the Department of Electrical, Electronic, and Information Engineering. From 2001 to 2008, he was the Associate Dean and then the Deputy Dean of the School of Engineering and from 2008 to 2012, he was the first Conjoint Dean of the School of Engineering and Mathematical Sciences, and the School of Informatics. In 2013, he was appointed as the Inaugural Dean of City Graduate School. He was appointed as a George Daniels Professor of scientific instrumentation in 2013, and to the Royal Academy of Engineering Research Chair in 2014.

He has authored or coauthored more than 700 refereed journal publications in main international journals and a similar number at key conferences. He has co-edited a five volume topical series on *Optical Fiber Sensor Technology*. He holds several patents for instrumentation systems for monitoring in industry using optical techniques. His research interests include the development and use of fiber optic and optical systems in the measurement of a range of physical and chemical parameters. His work has been sponsored by a number of organizations, including EPSRC, the EU, private industry, and charitable sources.

He is extensively involved with the work of the professional bodies having been Chairman of the Science, Education and Technology of the Institution of Electrical Engineers (now IET) and the Applied Optics Division, Institute of Physics and was the President of the Institute of Measurement and Control during 2000. He was on the Councils of all three of these professional bodies. His work is highly cited by his peers nationally and internationally. He was elected as the President of the International Measurement Confederation in 2014, serving from 2015 to 2018. He was elected to the Royal Academy of Engineering, the U.K. National Academy of Engineering, in 2008. He was the recipient of the Callendar Medal of the Institute of Measurement and Control in 1992, twice the Honeywell Prize for work published in the Institute's journal, the Sir Harold Hartley Medal in 2012 for distinction in the field of instrumentation and control, the Applied Optics Divisional Prize in 2010 for his work on optical sensing, and the Honorary Degree of Doctor of the University from the University of Oradea in 2014.